

Spiral Transformation for High-Resolution and Efficient Sorting of Optical Vortex ModesYuanhui Wen,^{1,*} Ioannis Chremmos,^{1,2,*} Yujie Chen,^{1,†} Jiangbo Zhu,³ Yanfeng Zhang,¹ and Siyuan Yu^{1,3,‡}¹*State Key Laboratory of Optoelectronic Materials and Technologies, School of Electronics and Information Technology, Sun Yat-sen University, Guangzhou 510275, China*²*Hellenic Electricity Distribution Network Operator S.A., Athens 11743, Greece*³*Photonics Group, Merchant Venturers School of Engineering, University of Bristol, Bristol BS8 1UB, United Kingdom* (Received 24 January 2018; published 11 May 2018)

Mode sorting is an essential function for optical multiplexing systems that exploit the orthogonality of the orbital angular momentum mode space. The familiar log-polar optical transformation provides a simple yet efficient approach whose resolution is, however, restricted by a considerable overlap between adjacent modes resulting from the limited excursion of the phase along a complete circle around the optical vortex axis. We propose and experimentally verify a new optical transformation that maps spirals (instead of concentric circles) to parallel lines. As the phase excursion along a spiral in the wave front of an optical vortex is theoretically unlimited, this new optical transformation can separate orbital angular momentum modes with superior resolution while maintaining unity efficiency.

DOI: [10.1103/PhysRevLett.120.193904](https://doi.org/10.1103/PhysRevLett.120.193904)

Light waves carrying orbital angular momentum (OAM), also known as optical vortices, possess a spiral phase structure in the form of $\exp(i\ell\theta)$, where θ is the azimuthal angle around the beam axis and the integer ℓ is the topological charge which translates to an OAM of $\ell\hbar$ per photon [1]. Either in the form of free-space vortex beams or optical fiber modes, OAM states of light with different topological charges are mutually orthogonal and thus constitute a high-dimensional state space that can be exploited to boost the information capacity in both classical [2–5] and quantum communication systems [6–8].

OAM states of light can be generated by a variety of techniques, such as spiral phase plates [9], spiral holograms [10], integrated microring resonators with embedded gratings [11], or by spin to OAM conversion [12]. Besides generation, a critical component of every OAM-based optical communication system is a mode sorter capable of efficiently separating different OAM modes in terms of power loss and intermodal cross talk. A number of relevant methods have appeared in the literature. Sorting schemes based on Mach-Zehnder interferometers [13] (see also Ref. [14] for radial modes) can theoretically achieve unity power efficiency but require multiple cascaded sorting stages and a complexity that increases with the number of sorted OAM modes. Similar complexity issues are presented by spatial mode multiplexers that require multiple successive phase modulations and Fourier transformations [15]. Another sorting method utilizes complex vortex gratings that impart different topological charges to beams of different diffraction orders [16,17]. The efficiency of this approach is, however, inherently limited to $1/N$, with N being the dimension of the underlying OAM state space. Efficiency and fabrication difficulties also exist with

integrated devices that sample a limited wave-front area of the OAM modes and require careful engineering of the involved optical waveguides [18]. Mode sorting based on the spin-to-OAM coupling in birefringent liquid crystals (q plates) has also been demonstrated—with, however, the requirement to discriminate between the overlapping radial distributions of the different modes [19].

A sorting method that is both efficient and simple is based on a ray-optics coordinate transformation [20]. Only two phase masks are required, the first for implementing the geometrical transformation and the second for collimating the output beam. The scheme is based on the familiar log-polar transformation in which log-polar coordinates in the input plane are conformally mapped to Cartesian coordinates in the output plane [21]. In this way, an input OAM mode with a spiral wave front $\exp(i\ell\theta)$ is transformed to a tilted plane wave front $\exp(i\ell x/\beta)$, where x is a Cartesian coordinate and β is a scaling parameter. OAM modes with different ℓ values are hence transformed to plane wave fronts with different tilt angles which can subsequently be focused to distinct positions in the focal plane of a lens, allowing them to be detected and processed as separate channels, as illustrated in Fig. 1. The experimental implementation of this scheme has been continuously improving, from using spatial light modulators (SLMs) [20] to custom refractive elements [22] and, recently, to compact mode sorters fabricated with electron beam lithography [23] and 3D laser printing [24].

The simplicity of OAM mode sorting based on the log-polar transformation comes at the cost of an inherent limitation in adequately separating adjacent OAM states, which is due to a significant overlap between their distributions in the output plane. The origin of this overlap is in the mathematical transformation itself. For an input

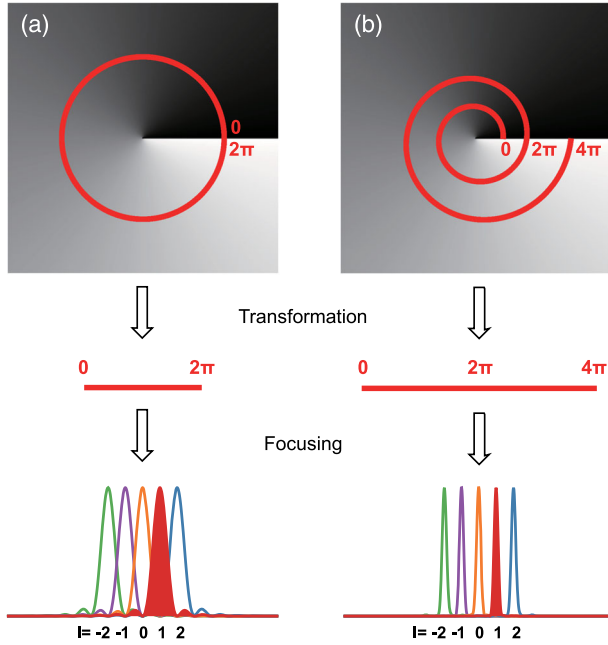


FIG. 1. Principle of (a) the log-polar transformation scheme, and (b) the introduced spiral transformation scheme for OAM mode sorting.

OAM mode with topological charge ℓ , the $2\pi\ell$ excursion of the phase around a complete circle in the transverse plane around the vortex axis is transformed to an equal phase excursion along a line segment in the output plane. After focusing, the cross section of the field amplitude profile in the Fourier plane resembles a sinc function that is shifted from the center by a wave number proportional to ℓ . Fourier analysis shows that the position of the sinc function equals $k_\ell = \ell/\beta$, while its width is $2/\beta$ (defined as the distance between the first two zeros on either side of the central maximum). The peaks of two adjacent OAM modes with topological charges ℓ and $\ell + 1$ are, therefore, separated by $k_{\ell+1} - k_\ell = 1/\beta$, which is only half the width of the sinc functions, resulting in significant power overlap between them and thus in limited discrimination resolution, giving rise to cross talk between the separated channels, as shown in Fig. 1(a). To alleviate this problem, post-transformation processing was proposed that artificially elongates the transformed output wave front by means of beam copying and stitching—at the cost, however, of a more complex optical setup and additional numerical effort for parametric optimization [25–27].

In this Letter, we take a fundamentally different approach to overcome the limitations of the log-polar OAM mode sorting scheme. We propose that *spiral transformations*, mapping spirals (instead of circles) to parallel lines, can be exploited toward OAM mode sorting with significantly higher resolution. As illustrated in Fig. 1(b), compared to the log-polar method, the proposed spiral transformation scheme provides a natural n -fold increase of the phase

excursion along the output wave front, where the number n of the spiral turns being imaged is limited only by the beamwidth of the input OAM mode. The extended output wave front is then mapped in the Fourier plane to a sinc function with the same shift, $k_\ell = \ell/\beta$, but with a width that is inversely proportional to the number of turns, $2/(n\beta)$, which translates to a significantly reduced overlap between adjacent OAM modes. Starting from first principles, we derive the condition for the existence of such spiral transformations. We specifically demonstrate the simplest analytical transformation of this kind that conformally maps logarithmic spirals to parallel lines, which is interestingly found to generalize the standard log-polar transformation. The theoretical predictions are verified through numerical simulations and an experiment.

To obtain the spiral coordinate transformation, we consider paraxial propagation of a light wave between an input plane (x, y) and an output plane (u, v) that is parallel to the input plane and located at a distance d . The mapping of point (x, y) to point (u, v) is given in the context of ray optics by the equations

$$Q_x = k \frac{u-x}{d}, \quad Q_y = k \frac{v-y}{d}, \quad (1)$$

where $Q(x, y)$ is the phase distribution in the input plane (imposed, in practice, by a phase mask), Q_x and Q_y are its partial derivatives with respect to the corresponding variables, and k is the free-space wave number. We now introduce the new coordinates (s, θ) in the (x, y) plane according to the equations

$$x = r(s, \theta) \cos \theta, \quad y = r(s, \theta) \sin \theta, \quad (2)$$

where (r, θ) represent the polar coordinates of the point (x, y) . The new coordinates (s, θ) can be considered as spiral-polar coordinates, where the parameter s indicates the particular spiral that the point (x, y) belongs to and the polar angle θ determines the position of the point on that spiral. Playing the role of a position parameter along a spiral of infinite length, the angle θ varies without restriction in $[0, \infty)$, which is already the first difference with the standard log-polar transformation where the angle is limited in the interval $[0, 2\pi)$. The shape of the spiral is determined by the function $r(s, \theta)$. For example, an Archimedean spiral can be expressed as $r(s, \theta) = s + a\theta$, and a logarithmic spiral as $r(s, \theta) = s \exp(a\theta)$, where $a > 0$.

Now consider the mapping of an input spiral $r(s, \theta)$ to an output straight line, which can be expressed as

$$u = u(s, \theta), \quad v = v(s). \quad (3)$$

These equations imply that the spiral labeled by the variable s can be mapped to a horizontal line in the output plane (parallel to the u axis), with the position u along that line generally depending on both s and θ . Spirals with different

parameters s are therefore mapped to parallel horizontal lines displaced in the vertical direction (parallel to the v axis) according to the function $v(s)$.

If the input phase distribution $Q(x, y)$ is to be a twice continuously differentiable function, we must have $Q_{xy} = Q_{yx}$. From Eq. (1), we have $u_y = v_x$, and due to Eq. (3),

$$u_s s_y + u_\theta \theta_y = v'(s) s_x, \quad (4)$$

which can be further rewritten in polar coordinates as

$$[u_s r_\theta - u_\theta r_s + v'(s)r] \cos\theta + [v'(s)r_\theta - u_s r] \sin\theta = 0. \quad (5)$$

This is the general condition imposed on the spiral transformation, which leads to a number of solutions $r(s, \theta)$ corresponding to different types of spirals. For reasons of simplicity and demonstration, in the following we pursue the simplest case, which follows from Eq. (5) by setting both factors of the trigonometric functions equal to zero and leads to

$$u_s = u_\theta \frac{r_s r_\theta}{r^2 + r_\theta^2}, \quad v'(s) = u_\theta \frac{r_s r}{r^2 + r_\theta^2}. \quad (6)$$

For a given spiral shape $r(s, \theta)$, Eqs. (6) relate the functions $v'(s)$, u_s , and u_θ , which have to be solved in order to yield the image (u, v) of the spiral in the output plane. However, since there are only two equations, one of the three unknown functions has to be determined by a separate requirement. For the OAM mode sorting purpose, it is desired to map the constant phase gradient along the azimuth of an input OAM mode, namely, $\exp(i\ell\theta)$, to a constant phase gradient along the u direction of the output mode, namely, $\exp(i\ell u/\beta)$. Hence, a linear relationship between θ and u is assumed, or $u_\theta = \beta$, where the constant β is the scaling parameter mentioned before. Under this assumption, the fraction about r in the right-hand side of the second equation of Eqs. (6) should be independent of θ , which leads to the solution of a logarithmic spiral $r(s, \theta) = s \exp(a\theta)$. Equations (6) can then be integrated to yield

$$u(s, \theta) = \frac{a\beta}{1+a^2} \ln\left(\frac{s}{r_0}\right) + \beta\theta, \quad v(s) = \frac{\beta}{1+a^2} \ln\left(\frac{s}{r_0}\right), \quad (7)$$

where we have arbitrarily chosen that the point $\theta = 0$ of the spiral with $s = r_0$ (an arbitrary positive constant) is mapped to $(0, 0)$. The transformation can be rewritten in the form of polar coordinates (r, θ) in the input plane

$$\begin{aligned} u(r, \theta) &= \frac{\beta}{1+a^2} \left[a \ln\left(\frac{r}{r_0}\right) + \theta \right], \\ v(r, \theta) &= \frac{\beta}{1+a^2} \left[\ln\left(\frac{r}{r_0}\right) - a\theta \right], \end{aligned} \quad (8)$$

where the relation between the polar angle $\theta \in [0, \infty)$ as a position parameter along a spiral and the Cartesian coordinates (x, y) is given in the Supplemental Material (SM) [28].

Equations (8) describe the simplest spiral transformation to be specifically demonstrated in this Letter. From a mathematical viewpoint, it is also interesting to find that this spiral transformation actually generalizes the standard log-polar mapping. Indeed, by introducing the complex variables $W = v + iu$ and $Z = x + iy$, Eqs. (8) can be written compactly as the conformal mapping between the Z (input) and W (output) complex planes,

$$W = \frac{\beta}{\sqrt{1+a^2}} e^{i\phi} \ln\left(\frac{Z}{r_0}\right), \quad (9)$$

where $\phi = \tan^{-1}(a)$. By setting $a = 0$, we have $\phi = 0$ and Eq. (9) reduces to the log-polar transformation. For some further analysis and a visualization of this new transformation, the reader is referred to the SM [28].

Having derived the analytical form of the spiral transformation [Eqs. (8)], we integrate the ray equations (1) to obtain the input phase distribution $Q(x, y)$, which reads

$$Q = \frac{k\beta}{d(a^2+1)} \left[(ax+y) \ln\left(\frac{r}{r_0}\right) + (x-ay)\theta - (ax+y) \right] - \frac{kr^2}{2d}. \quad (10)$$

This is the input phase required to map spirals of the input plane to parallel lines in the output plane after propagation by a distance d . The corresponding distribution $P(u, v)$ of the second, phase-correction element that is required to compensate for the phase acquired by the wave during propagation is given in the SM [28]. A typical example of these phase distributions is shown in Fig. 2(b) and compared to the log-polar case [Fig. 2(a)]. It is noted

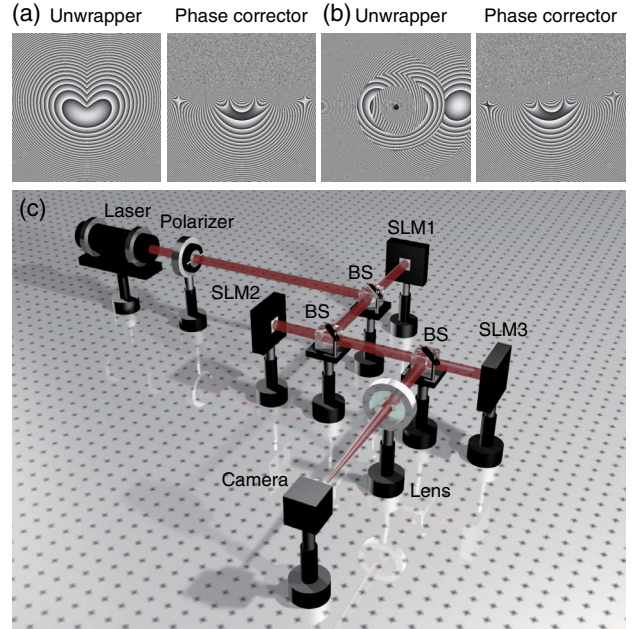


FIG. 2. Phase masks used for implementing (a) the log-polar and (b) the spiral transformation. (c) Schematic of the experimental setup. BS denotes beam splitter.

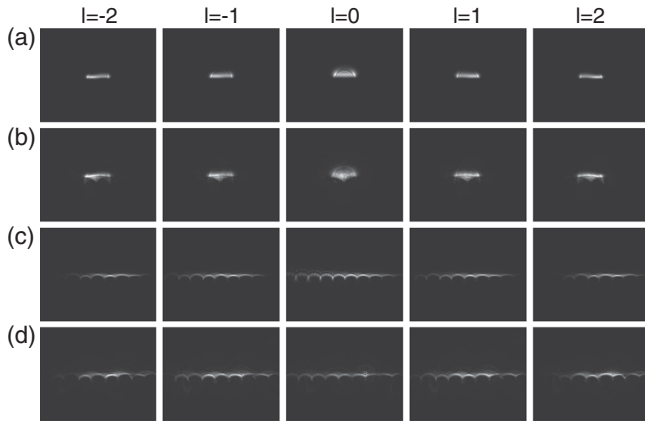


FIG. 3. (a),(c) Numerical and (b),(d) experimental intensity distributions of vortex beams with topological charges $-2 \leq l \leq 2$ transformed by (a),(b) the log-polar and (c),(d) the spiral transformation scheme. All images refer to the plane just after (or just before) the phase corrector [SLM3 in Fig. 2(c)] and have the same spatial scale.

that phase modulation with higher spatial resolution is generally required to implement the spiral transformation than with the log-polar transformation, and the resolution requirement is approximately proportional to the number of spiral turns, which, however, can still be easily fulfilled in practice by commercially available SLMs or other custom phase elements.

Our theoretical predictions for the performance of the spiral transformation in sorting OAM modes have been verified by numerical simulations and an experiment and compared to the standard log-polar transformation. The numerical simulations are based on the angular spectral decomposition of the diffracted waves using Laguerre-Gaussian beams as input OAM modes, while the corresponding experimental setup is shown in Fig. 2(c). The first SLM (SLM1) serves to generate the OAM modes from an initial Gaussian beam, while SLM2 (the *unwrapper*) and SLM3 (the *phase corrector*) implement the phase distributions $Q(x, y)$ and $P(u, v)$, respectively. The geometrical parameters of the transformation are chosen to ensure diffraction in the paraxial regime, with the typical values used being $d = 134$ mm, $2\pi\beta = 2$ mm, $r_0 = 1.1$ mm, and $2\pi a = \ln(1.6)$, at a telecommunication wavelength $\lambda = 1550$ nm.

Figure 3 summarizes the numerical and experimental results for vortex beams with different topological charges ($-2 \leq \ell \leq 2$) being transformed according to the log-polar [Figs. 3(a) and 3(b)] and the spiral [Figs. 3(c) and 3(d)] transformation principle. In the log-polar scheme, the input OAM modes are transformed to rectangular stripes of limited length $2\pi\beta = 2$ mm, while in the spiral scheme the OAM modes are mapped, as expected, to significantly longer lines, which reflects the number of spiral turns (about three turns on average, in this case) being mapped

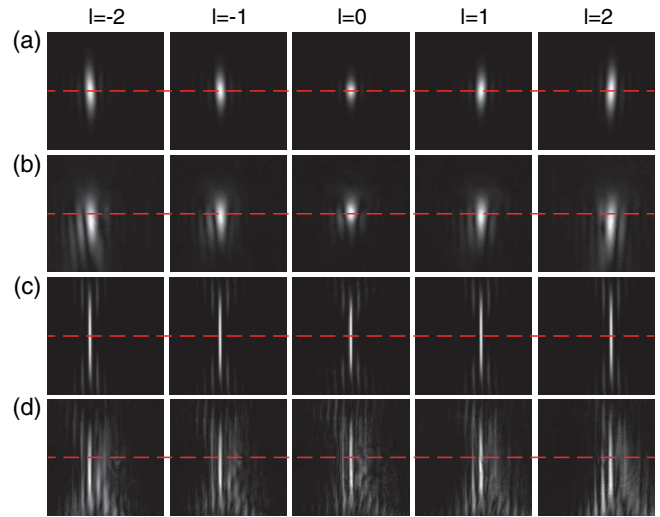


FIG. 4. (a),(c) Numerical and (b),(d) experimental intensity distributions of sorted vortex beams with topological charges $-2 \leq l \leq 2$ in the focal (Fourier) plane of the lens, based on (a),(b) the log-polar and (c),(d) the spiral transformation scheme. All images have the same spatial scale.

within the beamwidth of the input vortex mode. The agreement of the experimental results with the simulations, regarding the shape and the length of the transformed images, is quite satisfactory.

Figure 4 shows the numerical and experimental results of the eventually separated OAM modes ($-2 \leq \ell \leq 2$) for the two transformation schemes. Figure 5 depicts the intensity profiles of these modes in the horizontal direction along the dashed middle lines shown in Fig. 4. As expected for both schemes, OAM modes with different topological charges are horizontally displaced from the center by a shift proportional to their topological charge. The shift is the same in both schemes for modes with the same topological charge because both schemes employ the same scaling parameter β . For a focal distance $f = 0.5$ m, the

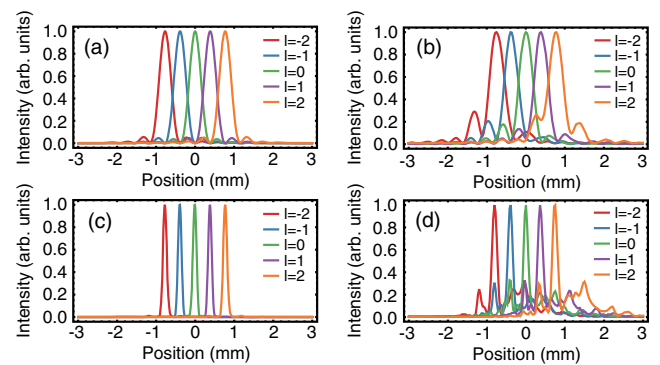


FIG. 5. Intensity profiles along the dashed middle lines in the images of Fig. 4 for different OAM modes. (a),(c) Numerical and (b),(d) experimental results for (a),(b) the log-polar and (c),(d) the spiral transformation scheme.

theoretical spacing between adjacent OAM modes is $\lambda f / (2\pi\beta) = 387.5 \mu\text{m}$, which is very close to the experimentally measured value in Fig. 5.

What is, however, most important about the results is the significant improvement in the separation of the OAM modes by the spiral transformation compared to the log-polar one. This is obvious either by comparing the numerical results of Figs. 5(a) and 5(c) or by comparing the experimental results of Figs. 5(b) and 5(d), where the sinc² profiles of the separated OAM modes in the spiral scheme are clearly narrower and less overlapping than the corresponding profiles of the log-polar scheme. The improvement can be quantified by using the concept of optical finesse, which is defined as the ratio of the spacing between adjacent OAM states over their average FWHM [27]. In our case, this indicator is approximately tripled, from 1.13 for the log-polar scheme to 3.48 for the spiral scheme in the simulation, and from 0.95 to 2.60 in the experiment. The slight difference between the numerical and experimental values results from beam broadening in the experiment. It is also noted that the experimental results seem to be affected by some stray light in the background, which is attributed to small errors in the 3D alignment of the SLMs, such as transverse displacement, rotation, and the distance between them, leading to imperfect phase correction in the output plane. Such problems can be overcome if the entire sorting scheme is arranged in a single device that comprises both the unwrapper and the phase corrector [23,24].

In summary, we have proposed a novel spiral transformation scheme for high-resolution OAM mode sorting. Starting from first principles, we have derived a general existence condition for such a transformation. Among the various possible types, we have specifically demonstrated a transformation which conformally maps logarithmic spirals to parallel lines and which has also been found to generalize the well-known log-polar transformation. The theoretical predictions have been verified through numerical simulations and an experiment, particularly the expected reduction in the overlap between adjacent sorted OAM modes compared to the log-polar scheme.

The new optical transformation scheme demonstrated in this work widens our views of the mathematical tools and concepts available toward efficient OAM mode sorting. Further possibilities and more sophisticated transformation schemes might emerge if similar concepts are sought beyond the regimes of ray optics and paraxial propagation, as, for example, in the context of wave optics, optical transformation media, and metamaterials.

This work is supported by the National Basic Research Program of China (the 973 Program under Grant No. 2014CB340000); the National Natural Science Foundation of China (NSFC) under Grants No. 61490715, No. U1701661, No. 11774437, No. 61323001, and No. 11690031; the Science and Technology Program of Guangzhou (Grants No. 201707020017 and

No. 201804010302); the European Union H2020 project ROAM; and Fundamental Research Funds for the Central Universities of China (SYSU) under Grant No. 17lgzd06. The authors thank Guoxuan Zhu (SYSU) for his helpful discussion of the experiment.

*These authors contributed equally to this work.

†Corresponding author.

chenyj69@mail.sysu.edu.cn

‡Corresponding author.

s.yu@bristol.ac.uk

- [1] L. Allen, M. W. Beijersbergen, R. J. C. Spreeuw, and J. P. Woerdman, Orbital angular momentum of light and the transformation of laguerre-gaussian laser modes, *Phys. Rev. A* **45**, 8185 (1992).
- [2] G. Gibson, J. Courtial, M. J. Padgett, M. Vasnetsov, V. Pas'ko, S. M. Barnett, and S. Franke-Arnold, Free-space information transfer using light beams carrying orbital angular momentum, *Opt. Express* **12**, 5448 (2004).
- [3] J. Wang, J.-Y. Yang, I. M. Fazal, N. Ahmed, Y. Yan, H. Huang, Y. Ren, Y. Yue, S. Dolinar, M. Tur, and A. E. Willner, Terabit free-space data transmission employing orbital angular momentum multiplexing, *Nat. Photonics* **6**, 488 (2012).
- [4] N. Bozinovic, Y. Yue, Y. Ren, M. Tur, P. Kristensen, H. Huang, A. E. Willner, and S. Ramachandran, Terabit-scale orbital angular momentum mode division multiplexing in fibers, *Science* **340**, 1545 (2013).
- [5] Y. Yan, G. Xie, M. P. J. Lavery, H. Huang, N. Ahmed, C. Bao, Y. Ren, Y. Cao, L. Li, Z. Zhao, A. F. Molisch, M. Tur, M. J. Padgett, and A. E. Willner, High-capacity millimetre-wave communications with orbital angular momentum multiplexing, *Nat. Commun.* **5**, 4876 (2014).
- [6] A. Mair, A. Vaziri, G. Weihs, and A. Zeilinger, Entanglement of the orbital angular momentum states of photons, *Nature (London)* **412**, 313 (2001).
- [7] J. C. García-Escartín and P. Chamorro-Posada, Quantum multiplexing with the orbital angular momentum of light, *Phys. Rev. A* **78**, 062320 (2008).
- [8] J. Leach, B. Jack, J. Romero, A. K. Jha, A. M. Yao, S. Franke-Arnold, D. G. Ireland, R. W. Boyd, S. M. Barnett, and M. J. Padgett, Quantum correlations in optical angle-orbital angular momentum variables, *Science* **329**, 662 (2010).
- [9] M. Beijersbergen, R. P. C. Coerwinkel, M. Kristensen, and J. P. Woerdman, Helical-wavefront laser beams produced with a spiral phaseplate, *Opt. Commun.* **112**, 321 (1994).
- [10] N. R. Heckenberg, R. McDuff, C. P. Smith, and A. G. White, Generation of optical phase singularities by computer-generated holograms, *Opt. Lett.* **17**, 221 (1992).
- [11] X. Cai, J. Wang, M. J. Strain, B. Johnson-Morris, J. Zhu, M. Sorel, J. L. O'Brien, M. G. Thompson, and S. Yu, Integrated compact optical vortex beam emitters, *Science* **338**, 363 (2012).
- [12] L. Marrucci, E. Karimi, S. Slussarenko, B. Piccirillo, E. Santamato, E. Nagali, and F. Sciarrino, Spin-to-orbital conversion of the angular momentum of light and its

- classical and quantum applications, *J. Opt.* **13**, 064001 (2011).
- [13] J. Leach, M. J. Padgett, S. M. Barnett, S. Franke-Arnold, and J. Courtial, Measuring the Orbital Angular Momentum of a Single Photon, *Phys. Rev. Lett.* **88**, 257901 (2002).
- [14] Y. Zhou, M. Mirhosseini, D. Fu, J. Zhao, S. M. Hashemi Rafsanjani, A. E. Willner, and R. W. Boyd, Sorting Photons by Radial Quantum Number, *Phys. Rev. Lett.* **119**, 263602 (2017).
- [15] G. Labroille, B. Denolle, P. Jian, P. Genevaux, N. Treppe, and J.-F. Morizur, Efficient and mode selective spatial mode multiplexer based on multi-plane light conversion, *Opt. Express* **22**, 15599 (2014).
- [16] N. Zhang, X. C. Yuan, and R. E. Burge, Extending the detection range of optical vortices by Dammann vortex gratings, *Opt. Lett.* **35**, 3495 (2010).
- [17] T. Lei, M. Zhang, Y. Li, P. Jia, G. N. Liu, X. Xu, Z. Li, C. Min, J. Lin, C. Yu, H. Niu, and X. Yuan, Massive individual orbital angular momentum channels for multiplexing enabled by Dammann gratings, *Light Sci. Appl.* **4**, e257 (2015).
- [18] T. Su, R. P. Scott, S. S. Djordjevic, N. K. Fontaine, D. J. Geisler, X. Cai, and S. J. B. Yoo, Demonstration of free space coherent optical communication using integrated silicon photonic orbital angular momentum devices, *Opt. Express* **20**, 9396 (2012).
- [19] E. Karimi, B. Piccirillo, E. Nagali, L. Marrucci, and E. Santamato, Efficient generation and sorting of orbital angular momentum eigenmodes of Light by thermally tuned q -plates, *Appl. Phys. Lett.* **94**, 231124 (2009).
- [20] G. C. G. Berkhout, M. P. J. Lavery, J. Courtial, M. W. Beijersbergen, and M. J. Padgett, Efficient Sorting of Orbital Angular Momentum States of Light, *Phys. Rev. Lett.* **105**, 153601 (2010).
- [21] W. J. Hossack, A. M. Darling, and A. Dahdouh, Coordinate transformations with multiple computer-generated optical elements, *J. Mod. Opt.* **34**, 1235 (1987).
- [22] M. P. J. Lavery, D. J. Robertson, G. C. G. Berkhout, G. D. Love, M. J. Padgett, and J. Courtial, Refractive elements for the measurement of the orbital angular momentum of a single photon, *Opt. Express* **20**, 2110 (2012).
- [23] G. Ruffato, M. Massari, and F. Romanato, Compact sorting of optical vortices by means of diffractive transformation optics, *Opt. Lett.* **42**, 551 (2017).
- [24] S. Lightman, G. Hurvitz, R. Gvishi, and A. Arie, Miniature wide-spectrum mode sorter for vortex beams produced by 3D laser printing, *Optica* **4**, 605 (2017).
- [25] M. N. O'Sullivan, M. Mirhosseini, M. Malik, and R. W. Boyd, Near-perfect sorting of orbital angular momentum and angular position states of light, *Opt. Express* **20**, 24444 (2012).
- [26] M. Mirhosseini, M. Malik, Z. Shi, and R. W. Boyd, Efficient separation of the orbital angular momentum eigenstates of light, *Nat. Commun.* **4**, 2781 (2013).
- [27] C. Wan, J. Chen, and Q. Zhan, Compact and high-resolution optical orbital angular momentum sorter, *APL Photonics* **2**, 031302 (2017).
- [28] See Supplemental Material at <http://link.aps.org/supplemental/10.1103/PhysRevLett.120.193904> for a further analysis of the spiral transformation.